Soft Matter

Measuring collective diffusion coefficients by counting particles in boxes

Journal:	*Soft Matter*
Manuscript ID	SM-ART-12-2024-001455.R2
Article Type:	Paper
Date Submitted by the Author:	15-Apr-2025
Complete List of Authors:	Carter, Adam; Sorbonne Universite Mackay, Eleanor; Oxford University Sprinkle, Brennan; Colorado School of Mines Thorneywork, Alice; University of Oxford, Physical and Theoretical Chemistry Marbach, Sophie; CNRS

Measuring collective diffusion coefficients by counting particles in boxes

Adam Carter,[1] Eleanor K. R. Mackay,[2] Brennan Sprinkle,[3] Alice L. Thorneywork,[2] and Sophie Marbach[1,*]

[1] *CNRS, Sorbonne Université, Physicochimie des Electrolytes et Nanosystèmes Interfaciaux, F-75005 Paris, France*
[2] *Physical and Theoretical Chemistry Laboratory, South Parks Rd, Oxford, OX1 3QZ UK*
[3] *Applied Math and Statistics, Colorado School of Mines, 1500 Illinois St, Golden, CO 80401*

(Dated: April 16, 2025)

The collective diffusion coefficient $D_{\rm coll}$ is a key quantity for describing the macroscopic transport properties of soft matter systems. However, measuring $D_{\rm coll}$ is a fundamental experimental and numerical challenge, as it either relies on nonequilibrium techniques that are hard to interpret or, at equilibrium, on Fourier-based approaches which are fraught with difficulties associated with Fourier transforms. In this work, we investigate the equilibrium diffusive dynamics of a 2D colloidal suspension experimentally and numerically. We use a "Countoscope" technique, which analyses the statistics of particle number counts $N(t)$ in virtual observation boxes of a series of microscopy images at equilibrium, to measure $D_{\rm coll}$ for the first time. We validate our results against Fourier-based approaches and establish best practices for measuring $D_{\rm coll}$ using fluctuating counts. We show that Fourier techniques yield inaccurate long-range collective measurements because of the non-periodic nature of an experimental image, yet counting exploits this property by using finite observation windows. Finally, we discuss the potential of our method to advance our understanding of collective properties in suspensions, particularly the role of hydrodynamic interactions.

Understanding the motion of an ensemble of particles, or collective motion, is a fundamental puzzle in soft matter. Outstanding questions in this area range from determining how molecules traverse a porous matrix [1–3] to learning how interactions between active or living particles trigger spontaneous group motion [4–7]. Here, a canonical example of collective motion is collective diffusion [8]. Yet for this most fundamental case we lack a full understanding even for systems with the simplest interactions, in part due to challenges associated with resolving collective dynamic properties from experimental microscopy data.

To understand the questions and challenges pertaining to the study of collective diffusion, we start by a brief overview of our understanding of self diffusion in particle suspensions. Following the seminal works of Stokes and Einstein [9], we understand the diffusion of a single particle suspended in a fluid as resulting from fluid molecules in thermal motion acting on the particle. This diffusion is typically characterised through the slope of the particle's mean-squared displacement,

$$D_{\rm self}(t) = \frac{1}{2d}\frac{\mathrm{d}}{\mathrm{d}t}\left\langle |\mathbf{r}(t+t_0) - \mathbf{r}(t_0)|^2 \right\rangle \qquad (1)$$

where $\mathbf{r}(t)$ is the particle position at time t in d dimensions and $\langle\cdot\rangle$ indicates averaging over all starting times t_0. At infinite particle dilution, $D_{\rm self}(t)$ provides the *bulk* or *free* diffusion coefficient $D_{\rm self}(t) \equiv D_0 = k_BT/\gamma$, where k_BT is the unit of energy and γ a friction coefficient (Fig. 1-a). When a particle diffuses in a suspension of particles, its *self* diffusion coefficient $D_{\rm self}(t)$ may differ from D_0 (Fig.1-b). It may be reduced due to interactions with neighbors, *e.g.* through a caging effect in the presence of repulsive interactions, or via hydrodynamic interactions [8]. In general, it depends on time. We define its short-time value, $D_{\rm self} = D_{\rm self}(t \simeq 0)$.

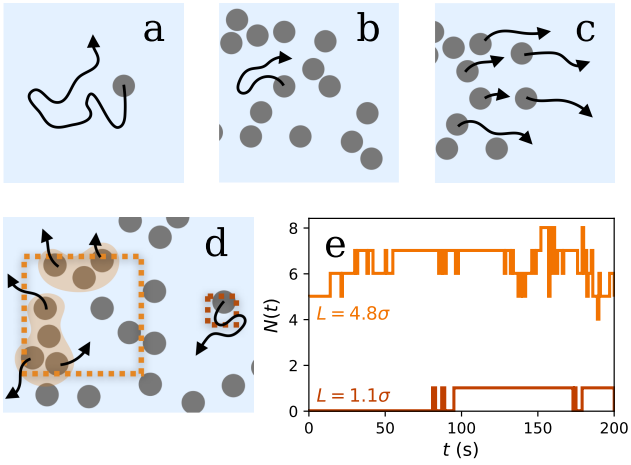

FIG. 1. **Inferring collective diffusion properties from counts**. Diffusion properties can refer to (a) the bulk or free diffusion coefficient of a particle D_0 suspended in a fluid, (b) the self-diffusion of a particle $D_{\rm self}$ in a suspension or (c) the collective diffusion coefficient of the suspension $D_{\rm coll}$, that describes the relaxation of a particle density gradient. (d) Here, we show how to measure $D_{\rm coll}$ from the relaxation of groups of particles at equilibrium in large virtual observation boxes on an image (orange). Counts in small boxes (red) probe individual motion. (e) The number of particles $N(t)$ in a box fluctuates due to individuals or groups of particles diffusing in and out of the box.

When a density gradient forms in a particle suspension, the so-called *collective* diffusion coefficient $D_{\rm coll}$ characterises the relaxation of the gradient, which is inherently a many particle behaviour (Fig. 1-c). Note

* sophie.marbach@cnrs.fr

that this coefficient is sometimes referred to as the transport diffusion coefficient, and we refer the reader to Ref. [10] for an overview. Most often, collective diffusion is defined via a *wavevector-dependent* diffusion coefficient $D(k,t)$ which characterizes the relaxation of a density fluctuation $\delta\rho = \rho(k,t) - \langle\rho\rangle$ at a wavelength k in a colloidal suspension as

$$\delta\rho(k,t) = \delta\rho(k,t=0)e^{-D(k,t)k^2t}. \quad (2)$$

In the large wavevector (short length scale) limit, $D(k,t)$ recovers the self diffusion coefficient, $D(k\to\infty,t) = D_{\rm self}(t)$. Conversely, in the vanishing wavevector (large length scale) limit, $D(k,t)$ gives the collective diffusion coefficient, $D(k\to 0,t) = D_{\rm coll}(t)$. In a few cases, *e.g.* for small density fluctuations or for pairwise additive interactions, the collective diffusion coefficient is independent of time [8, 11].

In contrast to self-diffusion, determining how individual interparticle interactions govern collective diffusion is complex. In general, collective diffusion is enhanced by interparticle interactions for hard-spheres, as moving particles push their neighbours, facilitating relaxation. A theoretical argument considering only pairwise interactions shows $D_{\rm coll} = D_{\rm self}/S(k=0)$, where $S(k=0)$ is the structure factor of the suspension at vanishing wavevector [8, 12]. At high particle densities in colloidal suspensions, $S(k=0)$ can be substantially smaller than 1, and therefore $D_{\rm coll}$ may indeed be significantly larger than D_0. This yields $D_{\rm self} \le D_0 \le D_{\rm coll}$ [8], highlighting how subtle collective diffusion is, even in a simple case. For hard sphere-like colloids in a suspension, an added complexity in verifying these theoretical models for how steric interactions influence collective diffusion is the inescapable presence of hydrodynamic interactions. In contrast to the case of self-diffusion, the effect of hydrodynamic interactions on collective diffusion coefficients is not well established and experimental results widely differ in assessing the role of hydrodynamic interactions on collective properties [13–23]. Methods to reliably measure $D_{\rm coll}$ are thus needed to shed light on collective motion.

Measuring collective diffusion coefficients from particle coordinates, both experimentally and numerically, is challenging. Since collective diffusion manifests out-of-equilibrium, several investigations explore the relaxation of a number density gradient [24–27]. However, such experiments are hard to repeat, because they require setting up the system out-of-equilibrium at the beginning of each experiment. In addition, as the density gradient relaxes, neither the gradient nor the local density is constant, which makes it hard to disentangle how $D_{\rm coll}$ depends on particle number density. Collective diffusion can also be probed in equilibrium, from density fluctuations that occur due to thermal motion. The relaxation of the density fluctuations is then investigated through the dynamic structure factor calculated in Fourier space [8]. Yet, Fourier transforms are computationally demanding and fraught with spurious features due to edge effects on microscopy images [28–30]. At equilibrium another strategy consists in probing the diffusion coefficient of the centre of mass of many particles [1–3, 10, 31, 32]. The collective diffusion coefficient is then proportional to the diffusion coefficient of the centre of mass [12]. Yet, obtaining a statistically meaningful trajectory for the centre of mass requires following a large group of particles for a substantial amount of time, which is experimentally challenging as particles continuously exit and enter the field of view. Even in simulations, only one trajectory is obtained, limiting statistical resolution.

Here, we establish a novel approach to measure collective diffusion coefficients experimentally and numerically by investigating the statistics of particle number counts $N(t)$ in virtual observation boxes at equilibrium (Fig. 1-d). The number $N(t)$ fluctuates due to particles diffusively entering and exiting a box (Fig. 1-e). For small observation boxes, fluctuations are dominated by individual particle motion. Large observation boxes sense collective motion since fluctuations also reflect the relaxation of transient groups of particles. In both cases, relaxation of fluctuations is linked to a characteristic time scale $T(L)$, which shows a non-trivial dependence on the size of the square box L. From this time scale, a length scale dependent diffusion coefficient has been defined, $D(L) \sim L^2/T(L)$, which is sensitive to $D_{\rm self}$ for small length scales, $D(L\to 0) = D_{\rm self}$, and to collective diffusion at large length scales $D(L\to\infty) = D_{\rm coll}$. This idea, termed the "Countoscope" (Sec. I), was proposed recently by some of us to probe self diffusion, yet its potential to probe collective diffusion coefficients has not been conclusively explored [23]. In this work, we determine best analysis practices and discuss perspectives to optimize this measurement (Sec. II). We compare our results with dynamic structure factor approaches, and find Fourier techniques yield inaccurate long-range collective measurements because of the non-periodic nature of an experimental image. In contrast, counting exploits finite images by paving the space with finite virtual observation boxes (Sec. III). Finally, we discuss how our methodology could provide further insights into the collective properties of suspensions(Sec. IV).

I. BRIEF INTRODUCTION TO THE COUNTOSCOPE WITH OVERLAPPED BOXES

A. Experimental system: 2D colloidal suspension near a wall.

We investigate the collective diffusive relaxation of a 2D suspension of colloids experimentally and numerically. We briefly restate the system's properties here and refer to Ref. [23] for details.

In experiments, particles, with effective hard sphere diameter $\sigma = 3.0\,\mu$m, which represent well a hard sphere

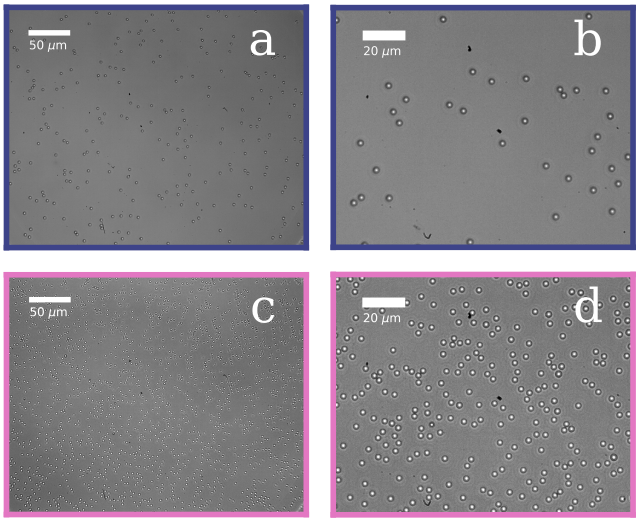

FIG. 2. **2D experimental hard-sphere system.** Optical images of (a,b, dark blue) the dilute $\phi = 0.02$ and (c,d, pink) the intermediate density $\phi = 0.11$ suspensions. (a,c) shows the entire field of view and (b,d) a cropped subset for visualization.

model [33, 34], are gravitationally confined in the z-direction to the base of a glass cell. Suspensions are imaged in the x-y plane using a custom-built inverted microscope – see SI section 1.1 for more details. Data is recorded at 2 fps and the total field of view is approximately $290\,\mu\text{m} \times 360\,\mu\text{m}$. Particle positions are acquired from images using standard particle tracking protocols [35, 36]. For simplicity, we explore here only two different packing fractions, corresponding to a dilute ($\phi = 0.02$) and intermediate density ($\phi = 0.11$) suspension – see Fig. 2. Note that while $\phi = 0.11$ lies far below the crystallisation transition for these systems, this packing fraction is sufficiently dense that interactions play an appreciable role. To obtain statistically accurate data over the long collective relaxation timescales we investigate, we acquire experimental data over 20 h. The optical stage and experimental conditions were carefully adjusted to avoid any significant drift over this long time scale (see SI section 1.1). At these packing fractions, the short-time self diffusion coefficient of particles can be calculated through Eq. (1) averaged over many particles, and gives $D_{\text{self}} = (0.048 \pm 0.001)\,\mu\text{m}^2/\text{s}$ at $\phi = 0.02$ and $D_{\text{self}} = (0.043 \pm 0.001)\,\mu\text{m}^2/\text{s}$ at $\phi = 0.11$.

In parallel, we conduct Brownian dynamics simulations representative of the experimental system. Simulation parameters are all set to their experimentally measured values, and steric forces are modelled using the hard potential in Eq. (31) of Ref. [37]. Hydrodynamic interactions between particles – both far field and lubrication interactions – are not accounted for in the simulation for simplicity. This allows for a direct comparison between the collective diffusion coefficient obtained from our simulations and that predicted by theory, which does not include hydrodynamics, to demonstrate the capabilities of our method. For the experiments, lubrication (near-field) interactions are not expected to play a significant role, as the mean distance between particles is large, greater than 3σ at the largest packing fraction $\phi = 0.11$. Far-field hydrodynamics do play a role as seen in the reduction of the short-time self-diffusion coefficient D_{self} at $\phi = 0.11$. As $D(k)$ and D_{coll} are expected to linearly depend on D_{self} at first order in the hydrodynamic interactions, we account for this by presenting most results renormalized by D_{self}. Finally, hydrodynamic lubrication between particles and the bottom glass wall is accounted for [37] through the value of D_0. This is reduced with respect to the value for a particle in the bulk by a factor consistent with theoretical predictions [37, 38]. Further numerical and simulation methods are described in SI section 1.2.

B. Number fluctuations in observation boxes.

For both experiments and simulations, we sample fluctuations in the number of particles $N(t)$ within square boxes of size $L \times L$ over time. $N(t)$ fluctuates between discrete values as a consequence of particles moving in and out of the box via diffusion (Fig. 1-e). We explore the statistical properties of this random number $N(t)$. We can compute the correlation function depending on the lag time t as

$$C_N(t) = \langle N(t+t_0)N(t_0)\rangle - \langle N\rangle^2 \tag{3}$$

where $\langle\cdot\rangle$ indicates an average over all boxes and time origins t_0 within the acquisition. For simplicity in the following we write $t_0 = 0$. Notice that when the lag time vanishes, $C_N(0) = \langle N^2\rangle - \langle N\rangle^2 \equiv \text{Var}(N)$. Another relevant quantity is the mean squared change in particle number,

$$\begin{aligned}\langle \Delta N^2(t)\rangle &= \langle (N(t) - N(0))^2\rangle \\ &= 2(\langle N^2\rangle - \langle N\rangle^2) - 2(\langle N(t)N(0)\rangle - \langle N\rangle^2) \\ &= 2\text{Var}(N) - 2C_N(t).\end{aligned} \tag{4}$$

Both statistical quantities will be useful to investigate as they characterize the dynamical relaxation of number fluctuations. In Fig. 3-a, we plot the mean squared change in particle number, $\langle \Delta N^2(t)\rangle$, for different box sizes in the dilute regime ($\phi = 0.02$). $\langle \Delta N^2(t)\rangle$ first increases in time. Starting from an initial condition with $N(0)$ particles in a box, as time goes by, one is more and more likely to see configurations where $N(t)$ is much higher or much smaller than $N(0)$, resulting in an overall increase of the squared difference $(N(t) - N(0))^2$ on average. Eventually, there is significant exchange between particles inside the box with those outside and we observe a plateau. The number of particles at long

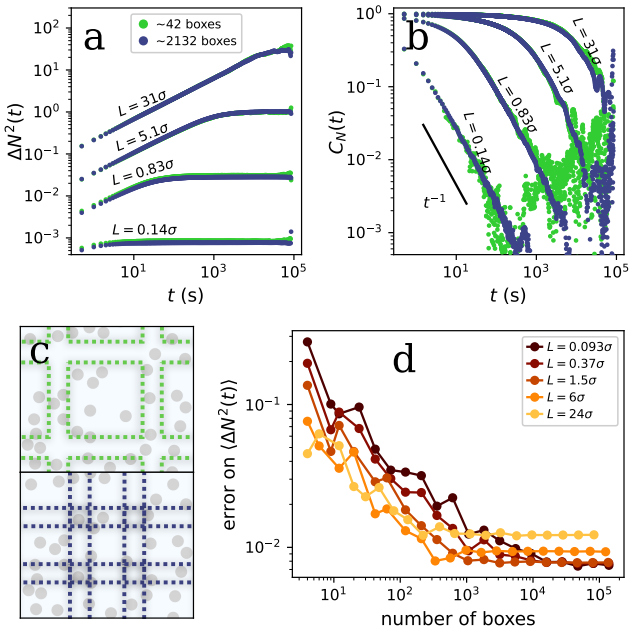

FIG. 3. **Importance of overlapping observation boxes.** (a) Number fluctuations $\langle \Delta N^2(t) \rangle$ and (b) correlation function $C_N(t)$ as a function of the lag time t for several box sizes for the dilute suspension $\phi = 0.02$. Experimental data. Legend is shared between a and b. (c) Schematic illustrating box overlapping. (d) Normalised average standard error on $\langle \Delta N^2(t) \rangle$ with respect to the number of observation boxes for different box sizes. The error is calculated by dividing the experimental data at $\phi = 0.02$ into 10 chunks in time, computing $\langle \Delta N^2(t) \rangle$ for each chunk, and finding the (averaged over time) standard error between chunks.

times is therefore uncorrelated with that in the initial configuration, *i.e.* $C_N(t) \simeq 0$ for long times (Fig. 3-b). From Eq. (4), the plateau corresponds to the variance $\langle \Delta N(t \to \infty) \rangle = 2\mathrm{Var}(N)$.

In Ref. [23], we established that number fluctuations can resolve the short-time self-diffusion coefficient of particles D_{self}. Indeed, at short times, fluctuations are dominated by individual particles entering or exiting boxes and satisfy $\langle \Delta N^2(t) \rangle \sim \sqrt{D_{\mathrm{self}} t / L^2}$. In a system with no interactions, the fluctuations relax over a timescale of about L^2/D_{self}. Yet for denser suspensions, over longer timescales, and especially in large boxes, the relative motion of groups of particles, or collective dynamics, should affect number fluctuations.

C. Overlapping boxes.

In this work, we aim to characterise the relaxation of number fluctuations, especially at large length scales – in large boxes – where collective dynamics are at play. Obtaining statistically accurate data over large boxes is inherently challenging, but can be optimized by carefully choosing how to distribute boxes spatially. With separated boxes (Fig. 3-c, green case), as in Ref. [23], statistical information is greatly reduced at large scales as fewer boxes fit on an image, with significant unused regions on an image. Instead, we propose to overlap sampling boxes (Fig. 3-c, blue case), significantly increasing the number of observation boxes. Qualitatively, overlapping boxes improve the resolution of the plateau of $\langle \Delta N^2(t) \rangle$ (Fig. 3-a), and significantly reduce noise on the long tails of the correlation function $C_N(t)$ (Fig. 3-b). This means that, although one obtains somewhat correlated data with overlapped boxes, the increased sampling is more important and improves statistical resolution.

To understand what degree of overlapped boxes yields the best statistics, we evaluate the average standard error on $\langle \Delta N^2(t) \rangle$ as we increase the number of boxes, and hence the amount of overlap between boxes (Fig. 3-d). The error decreases by an order of magnitude with increasing box numbers, confirming overlapped boxes significantly improve statistical accuracy. Eventually the error reaches a noise floor: as we pave space with boxes, boxes eventually become so overlapped that they are redundant and no more information is gained. Since this excessive overlap clearly happens with fewer boxes for larger boxes, the noise floor is reached with fewer boxes for large boxes than small ones. Overall, this suggests an upper limit for the number of boxes to use, which we take here to be 2000 boxes for our system parameters. We use this overlapping technique and bound in all future analysis.

II. COUNTOSCOPE TO MEASURE COLLECTIVE DIFFUSION PROPERTIES

We now use the Countoscope to investigate the relaxation of number fluctuations, focusing on how this relates to collective diffusion properties for large boxes. We do this by defining a box-size dependent coefficient $D(L)$, in analogy with $D(k)$ as discussed earlier. The two statistical quantities, $\langle \Delta N^2(t) \rangle$ and $C_N(t)$, allow us to explore two complementary methods to extract collective dynamics. In this section, we find $D(L)$ from a relaxation timescale $T(L)$, obtained by integrating the correlation function $C_N(t)$. We term this method the "timescale integral". In the SI (section 2) we present an alternative method, using a phenomenological fit of the number fluctuations $\langle \Delta N^2(t) \rangle$ to obtain $D(L)$. This second method is more suited to situations where the dataset length is limited, but it requires a phenomenological model of the effect at play, and is less accurate for sufficiently long datasets. We will compare results between an effectively non-interacting case, the dilute suspension at $\phi = 0.02$, and the intermediate density suspension at $\phi = 0.11$ where interactions modify behaviour. We will also explore differences between experimental data, simulations and theory. Importantly,

we will show $D(L)$ interpolates between two regimes, a regime in which self-diffusion dominates in small boxes (red in Fig. 1-d) and collective diffusion in large boxes (orange in Fig. 1-d).

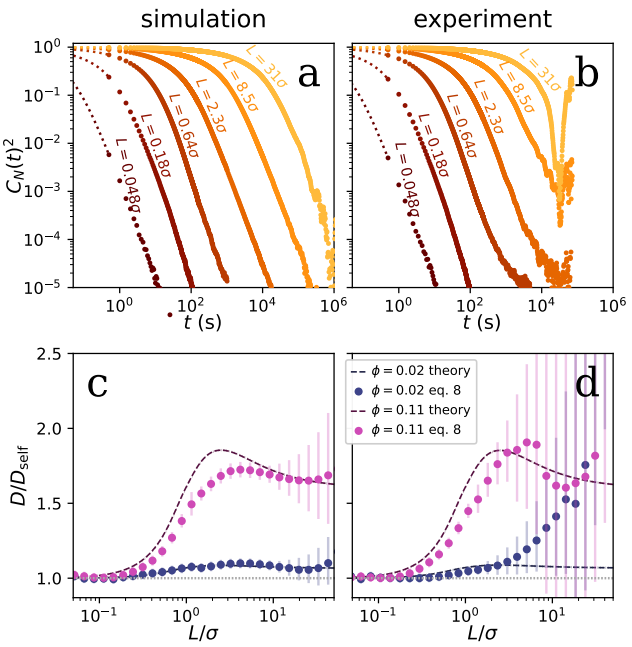

FIG. 4. **Decorrelation timescale of number fluctuations.** (a-b) Correlation functions $C_N(t)^2$ versus time for (a) simulations and (b) experimental data in the intermediate density $\phi = 0.11$ case. Box sizes go from small (dark red) to large (yellow). Dotted curves for $t \leq 0.5$ s represent short-time extensions to improve the accuracy of the integral of $C_N(t)^2$ on small boxes $L \leq \sigma$. (c-d) Diffusion coefficient $D(L) \propto L^2/T(L)$, where $T(L)$ is obtained from the integral of $C_N(t)^2$ from (a-b) for (c) simulations and (d) experimental data. Dashed lines correspond to the theory Eq. (5) (using also Eq. (S4)). Blue corresponds to the dilute regime, and pink the intermediate density. Error bars are propagated from 99% confidence intervals in the variance of $N(t)$ across all boxes and times.

A. Workflow of timescale integral method.

The timescale integral method is based on quantifying the relaxation time of the correlation function $C_N(t)$ (see Fig. 4-a and b). To quantify the timescale $T(L)$ of this decay, Ref. [23] suggested to integrate $C_N(t)$ as

$$T(L) = 2\int_0^\infty \left(\frac{C_N(t)}{C_N(0)}\right)^2 \mathrm{d}t = 2\int_0^\infty \left(1 - \frac{1}{2}\frac{\langle \Delta N^2(t)\rangle}{\mathrm{Var}(N)}\right)^2 \mathrm{d}t. \quad (5)$$

This definition means that for correlations that decay exponentially, T would represent the timescale of the decay as $C_N(t)/C_N(0) = \exp(-t/T)$. Note, here the unusual squaring factor in the integrand ensures that the integral converges, as the correlation function decays algebraically at long times, $C_N(t \to \infty) \sim 1/t$ [23, 39] (Fig. 3-b). Visually, $T(L)$ also roughly corresponds to the corner in the $\langle \Delta N^2(t)\rangle$ curves.

B. Scale-dependent diffusion coefficient $D(L)$ can probe D_{coll}

In the dilute regime, one can verify experimentally that T corresponds to the time to diffuse across the box, $T(L) \propto L^2/4D_0$; for dilute or non-interacting systems, rescaling time by L^2 is sufficient to describe the relaxation of fluctuations at all scales. At higher packing fractions, the time required to relax fluctuations does not solely depend on how long a single particle takes to diffuse over the length scale L (SI fig S3). Instead, it depends on the motion of multiple interacting particles.

We can relate T to a general diffusive phenomenon, by defining a diffusion coefficient dependent on the box size, as

$$D(L) = \alpha_T \frac{L^2}{4T(L)} \quad (6)$$

where $\alpha_T \simeq 0.56$ is a numerical constant, which can be obtained from a theory we describe below and whose lengthy expression is reported in Eq. (S16). We present $D(L)$ rescaled by D_{self} in Fig. 4-c and d for the 2 different packing fractions in this study, for simulations and experiments.

To gain insight on the behaviour of $D(L)$ we first investigate it with theory. Predictions for $C_N(t)$ can be obtained by describing the particle suspension with a stochastic density field theory (Dean-Kawasaki equations) [23, 40, 41]. In this theory, particle interactions are pair-wise interactions characterized via their structure factor $S(k)$. Thus, the theory is general in that it applies to any particle suspension with pair interactions. Here, we only include hard sphere interactions, thereby reproducing the ingredients of the simulations, and the expression of $S(k)$ is given by Eq. (S22). The theory is described in Ref. [23] and recapitulated in SI section 3.1. In the analytical curves (lines in Fig. 4-c and d), $D(L)$ plateaus for small boxes, increases, and eventually plateaus again. It can be shown analytically that for small boxes the timescale integral probes self diffusion, and for large boxes it probes collective diffusion

$$\begin{cases} D(L \to 0) = D_{\mathrm{self}}, \\ D(L \to \infty) = D_{\mathrm{coll}} = \dfrac{D_{\mathrm{self}}}{S(k=0)}. \end{cases} \quad (7)$$

We check the theory predictions by investigating $D(L)$ with our simulations and experiments. For both packing fractions, simulations closely follow the theory over

nearly the full range of box sizes: $D(L)$ plateaus for small boxes, increases, and then appears to plateau again. Experimental results also follow the theory up to around $L \gtrsim \sigma$ before hitting a divergent region. This divergence is due to limited statistical accuracy, and we discuss it further in Sec. II C. For small boxes $L \lesssim \sigma$, we find $D(L) \simeq D_{\text{self}}$ as expected, the box-size dependent diffusion coefficient probes individual motion. Collective motion then increases the effective diffusion coefficient $D(L)$ at intermediate lengthscales. In the simulations, $D(L)$ clearly reaches a plateau around $L \simeq 10\sigma$, which corresponds closely with the expected value of the collective diffusion coefficient D_{coll} of the suspension. This plateau is also apparent, though slightly less so in experimental data, and we discuss how to improve the measurement in Sec. II C. Overall, the timescale integral can indeed capture D_{coll} at large lengthscales.

At intermediate lengthscales, $L \simeq 2 - 4\sigma$, some discrepancies can be noticed between simulations, experiments and theory, for the largest packing fraction $\phi = 0.11$. As they do not appear for $\phi = 0.02$ these discrepancies arise because of particle interactions. In the theory, particle interactions are linearized assuming density fluctuations are small. From the difference between theory and simulations – which contain, as the theory, only hard sphere interactions – we can conclude that large density fluctuations arise at these intermediate lengthscales. Further discrepancies are observed between experimental data and simulations, which are likely arising from far-field hydrodynamic interactions.

Finally, experiments, simulations and theory highlight the presence of a peculiar maximum in the $D(L)$ curves in the intermediate density case $\phi = 0.11$ (pink), near $L \simeq 3\sigma$. This effect is quite subtle, and here we propose a qualitative explanation. For small box sizes, $L \ll \sigma$, one probes individual motion at small lengthscales, corresponding to a timescale much smaller than the mean time between collisions. For large box sizes, $L \gg \sigma$, one probes collective motion, *i.e.* the relaxation of transiently forming groups, at scales much larger than these transient groups, in essence at a mean-field level. For intermediate yet small box sizes, say $L \simeq \sigma$, one still probes individual motion but at a scale where a particle senses its neighbours. The interacting neighbours facilitate relaxation of number fluctuations, by pushing one another. This results in an increase of effective dynamics $D(L)$. This increased $D(L)$ can exceed D_{coll}, because the box is still small enough, $L \simeq \sigma$, that the magnitude of the number fluctuations that relax is still small on average. Schematically, at these scales one still investigates only individual particles that get effectively pushed out by their neighbours, resulting in a maximum of $D(L)$. We will comment on such behaviour further in Ref. [39].

C. Best practices for obtaining the timescale integral.

To perform the timescale integral accurately one must obtain an accurate estimate of the correlation function $C_N(t)$. Here, a significant challenge is to accurately calculate $\text{Var}(N)$. To obtain $C_N(t)$, the mean squared change in particle number $\langle \Delta N^2(t) \rangle$ is subtracted from its plateau, the variance $\text{Var}(N)$, as, according to Eq. (4), $C_N(t) = \left[\langle \Delta N^2(t) \rangle / 2 - \text{Var}(N) \right]$. Inaccurate estimates of $\text{Var}(N)$ thus result in divergences in $T(L)$, and on $D(L)$, as observed for large enough boxes in Fig. 4-c and d. The fact that $C_N(t)$ does not vanish smoothly for the boxes $L \geq 2\sigma$ in Fig. 4-b, also demonstrates that $\text{Var}(N)$ is not accurately resolved.

In general, 2D systems require long times to sample many different states, such that accurate estimates of $\text{Var}(N)$ are hard to access. A long-time scaling law can be obtained from the theory showing that $C_N(t)$ decorrelates slowly, as $1/t$ (see Fig. 3-b). This is a consequence of the fact that diffusing particles can always return to their starting point in 2D [39]. Resolving $\text{Var}(N)$ in 2D thus requires significantly long datasets, especially for larger boxes. Due to the slow decay of number correlations, we expect experiments need to be at least as long as the decorrelation time to resolve $\text{Var}(N)$ correctly. Indeed, for $L = 20\sigma$, the decorrelation time is roughly $T \simeq L^2/D_0 \simeq 23\,\text{h}$. Since this is about the duration of our experiments, this justifies that divergences appear in Fig. 4-d for $L \gtrsim 20\sigma$. Generally, this defines an upper box size that can be resolved in an experiment, as $L \lesssim \sqrt{D_0 T_{\text{exp}}}$ where T_{exp} is the experiment time.

Simulations without hydrodynamics can be conducted for long enough times that convergence in time is not an issue. Yet, we find reliable variance estimates are also hard to access for large boxes. We identify that better estimates of $\text{Var}(N)$ may be obtained by increasing the size of the periodic simulation box L_x (see SI Fig S6). Indeed, collective dynamics loop back onto themselves via the simulation's periodic boundaries, and hence large simulation boxes are needed for accurate resolution. This defines an upper box size that can be resolved in a simulation, as $L \simeq 0.3 L_x$. Here we have $L_x = 1280\,\mu\text{m}$ and so on boxes smaller than $L \lesssim 130\sigma$, accurate resolution is possible, which is apparent in Fig. 4-c. Finally, we note that, in this work, we take the variance as an average over all boxes and all times. To estimate the variance from such time-correlated data, other strategies such as bootstrapping could be used [42], or fitting the distribution of particles in a box. However, we find that our dominant source of error is not the method to estimate the variance but rather (*i*) lack of long time data in experiments, or (*ii*) lack of large simulation box in simulations.

The length of the dataset is also important in that, to integrate $C_N(t)$, one must have data over long enough time periods. During integration, the decay at long

times could be in part improved by replacing the long-time noisy data points with long-time theory-informed extensions, fitted to the experimental data [23]. However, in our experimental system, our dominant limitation is in resolving $\mathrm{Var}(N)$ and not lack of long-time data (SI Fig. S4). For boxes $L \lesssim 0.3\sigma$, the correlation function decays so quickly that our imaging timestep can not capture the early time decay, and hence $T(L)$ is incorrectly estimated. To circumvent this, we match our first experimental data point $C_N(\Delta t)$ where $\Delta t = 0.5$ s, is our experimental time, with a short time-small box formula in Eq. (S1) obtained via the theory, and integrate the short time extension over $[0, \Delta t]$ (see dotted coloured lines in Fig. 4-a and b for $t \leq 0.5$ s). This short time extension is added on all box sizes but only makes a significant difference on box sizes $L \lesssim \sigma$ where the decay of the correlation function is otherwise too fast to be captured by data.

III. COMPARISON TO A COMMON FOURIER-BASED APPROACH

To assess the performance of the Countoscope, we compare our results to another approach to calculate D_{coll} at equilibrium. Centre of mass approaches have low statistical resolution, and thus we rather focus on a Fourier-based approach for benchmarking.

A. Dynamic structure factors

A common approach to characterize the relaxation of diffusion processes at several scales is to analyze dynamic structure factors $F(k,t)$ for a given wavenumber k after a time interval t. The dynamic structure factor is also referred to as the intermediate scattering function [8]. Formally, it is defined in Fourier space as the correlation function of the Fourier-transformed densities, $F(k,t) = \langle \hat{\rho}(\boldsymbol{k},t)\hat{\rho}^{\star}(\boldsymbol{k},0)\rangle/N_p$ where N_p is the number of particles of the suspension. Each particle indexed by μ has 2D coordinates given by $\boldsymbol{r}_\mu(t) = (x_\mu(t), y_\mu(t))$, and one can equivalently rewrite

$$F(k,t) = \frac{1}{N_p}\sum_{\mu,\nu=1}^{N_p}\left\langle e^{i\boldsymbol{k}\cdot(\boldsymbol{r}_\mu(t)-\boldsymbol{r}_\nu(0))}\right\rangle \tag{8}$$

where we assumed the system is rotationally invariant such that F only depends on $k = |\boldsymbol{k}|$. At time zero, F is equal to the static structure factor $F(k, t=0) = S(k)$. Calculating $F(k,t)$ via Eq. (8) is also called the direct method [43].

The dynamic structure factor $F(k,t)$ characterizes how the structure of the fluid evolves from a given state. Within linear response, *i.e.* assuming density fluctuations are small, the structural dynamics are fully described by a diffusion coefficient in Fourier space $D(k,t)$ such that

$$f(k,t) \equiv \frac{F(k,t)}{S(k)} = \exp\left(-D(k,t)k^2 t\right). \tag{9}$$

Large wavenumbers refer to motion at small scales and hence correspond to individual motion, so we expect $D(k\to\infty,t) = D_{\mathrm{self}}(t)$. The limit of small wavenumbers in turn describes collective motion, by definition, $D(k\to 0,t) = D_{\mathrm{coll}}(t)$.

It is important to note that the dynamic structure factor bundles two contributions: correlations between a given particle at a given point in time with *itself* at a later time $F_s(k,t)$, and correlations between *distinct* particles at different times $F_d(k,t)$. This means $F(k,t)$ can be rewritten as

$$\begin{aligned} F(k,t) &= F_s(k,t) + F_d(k,t) \\ &= \frac{1}{N_p}\sum_{\mu}^{N_p}\left\langle e^{i\boldsymbol{k}\cdot(\boldsymbol{r}_\mu(t)-\boldsymbol{r}_\mu(0))}\right\rangle \ldots \\ &\quad + \frac{1}{N_p}\sum_{\mu\neq\nu}^{N_p}\left\langle e^{i\boldsymbol{k}\cdot(\boldsymbol{r}_\mu(t)-\boldsymbol{r}_\nu(0))}\right\rangle. \end{aligned} \tag{10}$$

The relaxation of the self part is entirely dictated by the self diffusion coefficient, as $F_s(k,t) = \exp\left(-D_{\mathrm{self}}k^2 t\right)$. In principle, D_{self} depends on time.

Turning now to the full dynamic structure factor, by inverting the decay of $f(k,t)$, one can obtain $D(k,t)$ linked to collective dynamics. So far we have kept a dependence of $D(k,t)$ on time, yet to simplify data analysis, for now, we will focus on short times, i.e., $D(k) = D(k, t \simeq 0)$, as data is generally better resolved at short times. In practice, this involves inverting Eq. (9) at the first (non zero) time point. In simulations and in the theory, we only consider hard sphere interactions, which are clearly pairwise additive and hence the collective diffusion coefficient is expected to be independent of time [11]. In experiments, the collective diffusion coefficient also appears to be independent of time, which may be a result of density fluctuations being small at the investigated packing fractions [8]. In the SI, we distinguish short and long time regimes, and show similar results overall (SI Fig. S6).

B. Divergence artefact of the dynamic structure factor for $k \to 0$.

The dynamic structure factor $F(k,t)$ is computed via Eq. (8) at various wavelengths k for the dilute suspension, $\phi = 0.02$, and shown in Fig. 5-a. From this we obtain $D(k)$ for all relevant wavelengths as presented in Fig. 5-b (diamonds). Surprisingly, for this dilute suspension we notice a clear divergence at small wavelengths of $D(k)$. Note that this divergence is not visible in the self diffusion coefficient D_{self} extracted in a similar way from $F_s(k,t)$ (Fig. 5-b, crosses). We do not expect such changes in the

collective diffusion coefficient $D(k \to 0)$ for such a dilute suspension.

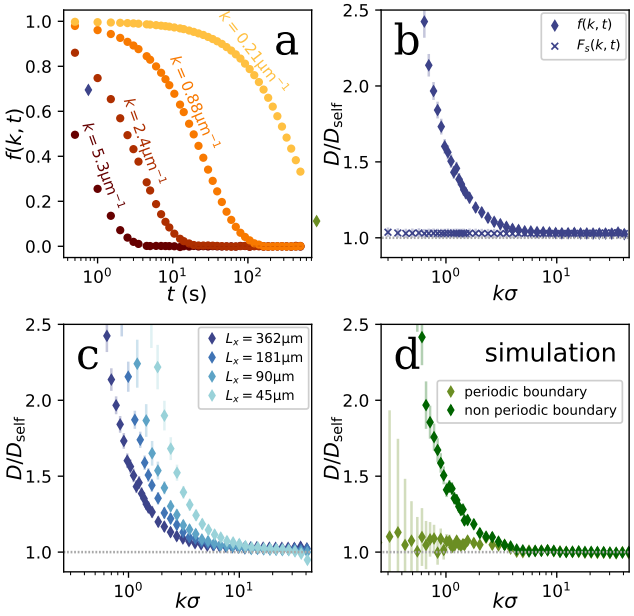

FIG. 5. **Challenges in resolving Fourier space relaxation from experiments at $\phi = 0.02$.** (a) Examples of dynamic structure factors $f(k,t)$ at different wavenumbers k. (b) Obtained $D(k)$ from first-point inversion of $f(k,t)$ and $F_s(k,t)$. (c) $D(k)$ from $f(k,t)$, but for cropped microscopy images. L_x as given in legend, L_y was picked to preserve aspect ratio of the field of view. (d) $D(k)$ from $f(k,t)$ from simulations with periodic and non-periodic boundary conditions. The numerical field of views are taken to be the same size. This subplot is repeated for the intermediate density case in SI Fig. S10. Error bars are propagated from the standard error in the value of $f(k,t)$ across all time origins.

To unravel the origin of this peculiar artefact, we conduct the analysis again on modified versions of the experimental data. First, we trim the duration of our experimental data, and plot $D(k)$ for different trimmed lengths, and find no significant difference (see SI Fig. S7). The artefact is thus not due to a lack of statistics. Second, we crop experimental movies, effectively reducing the effective field of view (L_x, L_y). The divergence in $D(k)$ is significantly affected by cropping: occurring at larger wavenumbers for smaller images, see Fig. 5-c. Typically, the divergence starts for k values such that $k \lesssim 2\pi/(L_x/10)$. This hints that the artefact originates from edge effects. Finally, we also compute $D(k)$ from simulation data, see Fig. 5-d (light green), and do not find the divergence.

The fundamental difference between experiments and simulations is that the simulated data has periodic boundary conditions. To mimic the experimental situation, we run a simulation on a much larger simulation box and do the $D(k)$ analysis on a cropped subset of the data, see Fig. 5-d (dark green). Under these simulated non-periodic boundary conditions, we recover a similar divergence in $D(k)$ as found experimentally. This demonstrates that the absence of periodic boundary conditions is at the origin of the artefact. The resolution of the dynamic structure factor is thus intrinsically limited by the finite field of view of the experiment.

While a detailed investigation of why this artefact appears is beyond the scope of this work, edge effects are its roots. Edge effects are common on Fourier transforms of images, where numerous techniques have been developed to limit related artefacts [28, 30]. Such techniques are not directly applicable to discrete particle positions, and hence to the computation of $F(k,t)$ via Eq. (8), yet motivate perspectives for improvement. To conclude, we simply raise caution and stress that for experimental data with observation windows of size L_x, k should be restricted such that $2\pi/k \lesssim 0.1 L_x$ when probing dynamic behaviour.

C. Results for $D(k)$ in a intermediate density suspension.

We now investigate the wave-number dependent $D(k)$ for the intermediate density suspension $\phi = 0.11$. To relate to our previous results obtained via the Countoscope, we present data as $D(k = 2\pi/L)$, effectively flipping the x axis horizontally. Fig. 6-a shows the results from simulation compared to the theoretical prediction $D(k) = D_{\text{self}}/S(k)$ (dotted lines in Fig. 6). Simulations without hydrodynamics perfectly reproduce the theory, and plateau to the collective diffusion coefficient D_{coll} as expected. Crucially this confirms the validity of our analysis scheme. Distinct features appear in $D(k)$ at the higher packing fraction at lower wavenumbers. In particular, we notice a minimum in $D(k)$ around $L \simeq \sigma$ $(\simeq 2\pi/k)$. The scale-dependent diffusion coefficient $D(k)$ is quite sensitive to the fluid's structure at different wavelengths, as expected from $D(k) \sim 1/S(k)$. The maximum in $S(k)$ (see Fig. S2), corresponding to ordering at increased packing fractions, thus corresponds with a minimum in $D(k)$, the so-called De Gennes narrowing [44]. This interpretation can be checked by overlapping the theoretical prediction $D(k) = D_{\text{self}}/S(k)$ on simulation and experiments (dotted lines in Fig. 6).

In contrast, sharp discrepancies arise between experimental data and theory for large lengthscales $L \gtrsim 3\sigma$ (Fig. 6-b). This divergence occurs at a similar lengthscale for experimental data at both $\phi = 0.11$ and $\phi = 0.02$, suggesting it is in both cases a consequence of the artefact discussed above. As such, beyond this value of k, interpretation of the data is ambiguous. Nonetheless, at lower wavenumber, the distinct features linked to De Gennes narrowing for the higher packing fraction are accurately resolved in $D(k)$ for the experiment. Divergence of $D(k)$ in previous works has been attributed to hydrodynamic corrections [19–

21]. Unfortunately, this reported behaviour arises for wavelengths where the divergence artefact in $D(k)$ kicks in for our results, and before the theory even reaches the D_{coll} plateau. To deconvolve hydrodynamic contributions from this artefact is beyond the scope of our work. Yet, several strategies are worth mentioning. On the experimental side, one could use wider fields of view to increase the range of relevant L lengths or design de-aliasing techniques [28, 30]. Simulations including hydrodynamic interactions between particles could be conducted [23, 37] and compared with simulations with purely steric interactions as well, but require intense computational resources.

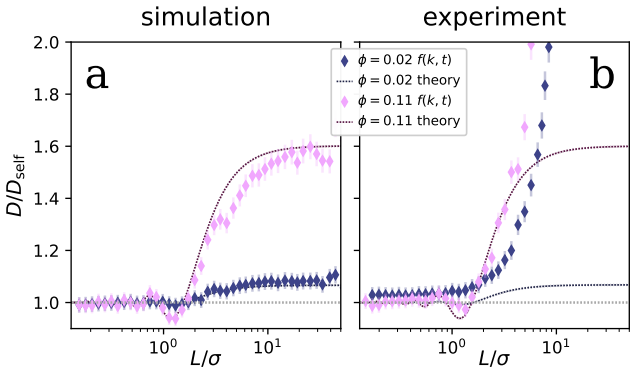

FIG. 6. **Relaxation of dynamic structure factors.** $D(L = 2\pi/k)$ for $\phi = 0.02$ (blue) and $\phi = 0.11$ (pink) obtained from short time analysis of the dynamic structure factor in (a) simulations and (b) experiments. Theory lines correspond with $D(k) = D_{\text{self}}/S(k)$ with $S(k)$ given in Eq. (S22). The divergence for $L \gtrsim 3\sigma$ in (b) corresponds to non-periodic boundaries as discussed in Fig. 5 and in the text. Error bars are propagated from the standard error in the value of $f(k,t)$ across all time origins.

D. Countoscope versus Fourier-based approaches

The features observed in $D(k)$ via the investigation of the dynamic structure factor are reminiscent of features of $D(L)$ inferred from the Countoscope. We compare the two approaches by overlapping $D(k)$ and $D(L)$ for simulations and experiments in the intermediate density regime $\phi = 0.11$ (Fig. 7). Overall, the fluid's structure is quite apparent on $D(k)$, and less so on $D(L)$. Curiously the maximum in $D(L)$ occurs at a similar lengthscale to the minimum in $D(k)$, a behaviour which would require further investigation at different packing fractions to be confirmed. The increase in the scale-dependent diffusion coefficient occurs at different scales: counting is sensitive to collective effects typically for $L \gtrsim \sigma$ while one must wait for $2\pi/k \gtrsim 5\sigma$ for collective effects in $D(k)$, demonstrating the sensitivity of counting.

Based on simulation data, we find counting can estimate the collective diffusion coefficient D_{coll} on large boxes. Indeed, in Fig. 7-a, we observe $D(k \to 0) = D(L \to \infty) = D_{\text{coll}}$. The measurement of the collective diffusion coefficient D_{coll} via the Countoscope or the dynamic structure factor approach are thus equivalent. As a periodic methodology, the Fourier-based approach on simulation data does not appear to diverge at large length-scales, compared to the Countoscope. Although the divergence is not apparent at the length scales presented in Fig. 7-a, it is apparent at larger length scales (SI Fig. S7). Nonetheless, one should keep in mind that finite-simulation size effects can still affect the plateau reached by $D(k)$ significantly (SI Fig. S7). As a Fourier methodology, dynamic structure factors access larger lengthscales than counting on periodic simulation data.

In experiments, it is hard at this stage to compare the limiting behaviour of $D(L)$ and $D(k)$ for $L \to \infty$ or $k \to 0$ due to the artefact divergence in $D(k)$. However, in experiments, counting provides information on $D(L)$ at much larger lengthscales than $D(k)$. Improving variance estimates would eventually increase the timescale integral's accuracy and decrease errors from the counting technique at the largest lengthscales. For $D(k)$, however, the system will always stay non-periodic and the divergence may be harder to fix. As a real-space methodology, counting is more robust on non-periodic experimental data than Fourier-based approaches.

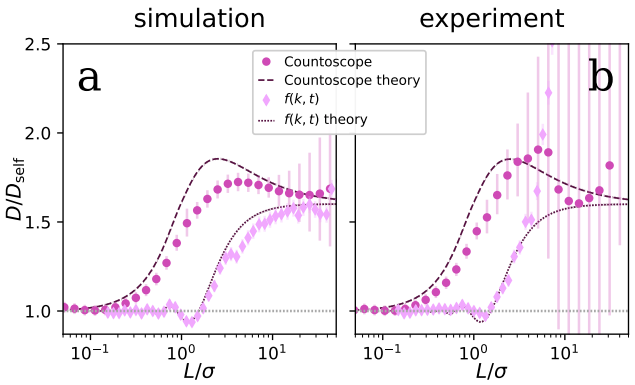

FIG. 7. **Comparison of Countoscope versus Fourier-space approaches:** via $D(L)$ computed via the timescale integral (dots) and $D(k = 2\pi/L)$ computed via the early-time fit of the dynamic structure factor (diamonds), for (a) simulations and (b) experiments for the highest packing fraction $\phi = 0.11$. Theory lines correspond with Eq. (6) for the Countoscope and $D(k) = D_{\text{self}}/S(k)$ with $S(k)$ given in Eq. (S22) for the Fourier approach.

IV. DISCUSSION AND CONCLUSION

In this work, we have shown how to infer collective diffusion properties at various spatial lengthscales by counting particles in boxes. The box-size dependent diffusion coefficient $D(L)$ can be obtained via time

integration of the correlation function of particle numbers in a box $\langle N(t)N(0)\rangle$. $D(L)$ converges to the self diffusion coefficient in small boxes $D(L \to 0) = D_{\text{self}}$. In large boxes, it probes the collective diffusion coefficient $D(L \to \infty) = D_{\text{coll}}$, as confirmed via a comparison between theory and simulations and investigation of the dynamic structure factor. For experiments, accurately determining $D(L)$ for large length scales is hindered by difficulties in determining the variance of the number fluctuations. However, we have found Fourier approaches, such as the dynamic structure factor, also struggle at large length scales due to the finite field of view of microscopy images, which leads to unphysical divergences of $D(L)$ at large wavelengths. In contrast, counting exploits finite fields of view by deliberately paving the image with finite observation boxes and could be made more accurate with an improved estimate of $\text{Var}(N)$. Finally, $D(L)$ informs on collective dynamics at all spatial scales L, allowing us to broadly investigate collective properties of suspensions.

While our investigation was centred on a 2D colloidal suspension, it introduces a general tool to infer the collective properties of suspensions from microscopy images. Indeed, the formalism applies to any quasi-2D experimental scenarios where particle coordinates can be obtained. Beyond that, we anticipate the Countoscope to be applicable in 3D. Given 3D particle coordinates, one can readily calculate number fluctuations in a 3D box, and then perform correlations, and the timescale integral. Interpretation of the results would be facilitated with further theory, which is *a priori* feasible with the current theoretical model [45]. However, 3D experimental setups often involve further complexities which remain to be accounted for in this context, and we leave this for further investigation.

We anticipate that our method could shed light on the effect of hydrodynamic interactions in colloidal suspensions, in particular for quasi 2D suspensions near walls, which occur quite commonly in soft matter systems. Previous theoretical and experimental investigations of quasi 2D geometries have suggested that long-range correlations between particles can enhance collective motion dramatically, resulting in a divergence of $D(k)$ at large wavelengths [18–22, 49–51]. This is at odds with bulk 3D systems, where hydrodynamic interactions reduce the value of D_{coll} [16–18]. Interestingly, we find in our experimental data that a divergence on $D(k)$ can be linked to edge effects, and thus potential effects of hydrodynamic interactions are hidden. In contrast, on experimental data for $D(L)$, we find no evidence for a divergence, however the error bars in our data at large length scales are very large. Beyond the artefact divergence, which could also be at play in previous works, discrepancies could originate from diverse physical factors. At higher packing fractions, up to $\phi \simeq 0.6$, we expect hydrodynamic effects could be more important [23]. The geometry of our system consists of particles at a single wall as opposed to a fluid-fluid interface or between two closely-spaced walls [18–22, 49], and geometry is known to significantly influence the range over which hydrodynamic interactions decay [52, 53]. The decay of hydrodynamic interactions could also be a transient short-time effect, requiring further interpretation of D_{coll} as a time-dependent property [13]. In more complex cases such as these, it remains an open question to identify whether fluctuating counts are sensitive to short or long time collective properties.

More generally, we stress that to obtain accurate quantification of collective properties, significant data sets are required, both in time and spatially: our experimental data sets are 100 times larger than the particle size, and more than 1000 times longer than the time to diffuse across a particle's diameter and only nearly capture D_{coll}. Given that wide fields of view are necessary to resolve motion at large spatial scales, for dense systems in particular trajectory reconstruction may no longer be feasible [35, 54, 55]. For the investigation of collective effects, this is not an issue as both counting or dynamic structure factors $F(k,t)$ do not require trajectories (Table I). In that sense, counting fills a gap in the field, as the real-space equivalent of $F(k,t)$. Density fluctuations are also investigated in real space through intensity fluctuations of scattered light, via Fluorescence Correlation Spectroscopy (FCS) [46] or Dynamic Light Scattering (DLS) [47]. In contrast with these techniques, we explicitly count numbers, avoiding the link between scattered intensities and particle numbers which is especially ambiguous at high densities [56, 57]. More importantly, the Countoscope is not restricted to a given lengthscale, unlike *e.g.* FCS which analyzes the scattered light of a given illuminated region. This suggests exploring intensity correlations in real space on virtual boxes of an image, a form of "intensity Countoscope". Again, this would fill a gap in the field, as the real space equivalent of Differential Dynamic Microscopy [48].

Finally, we hypothesize that probing number correlations at different scales could inform us about more diverse collective transport properties, beyond diffusion. For instance, in active matter systems, either synthetic or biological, peculiar features are common in static number fluctuations: "Giant" number fluctuations, where $\alpha > 0$ in the scaling $\langle N^2\rangle - \langle N\rangle^2 \sim N^{1+\alpha}$, indicate long-range organization, as found in bacterial aggregates and active matter [58–66]. Likely, investigating the dynamic counterpart of these static fluctuations, through the decorrelation time $T(L)$ of number fluctuations at different scales could help us characterize collective motile states, and perhaps shed light on how they emerge from specific interparticle interactions [6, 7].

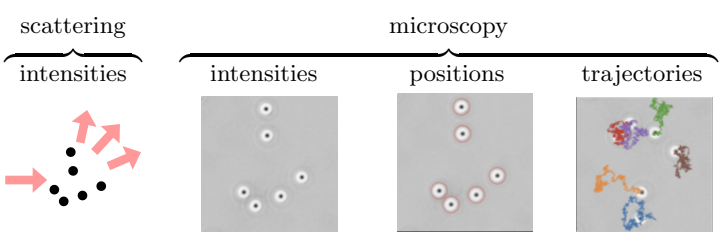

Real-space	FCS, DLS	Intensity Counting	Countoscope	MSD
Fourier-space	XPCS, DLS	DDM	$F(k,t)$	$F_s(k,t), F_d(k,t)$

TABLE I. Comparison of different techniques for analyzing particle dynamics in scattering and microscopy experiments. FCS = Fluorescence Correlation Spectroscopy [46], DLS = Dynamic Light Scattering [47], XPCS = X-ray Photon Correlation Spectroscopy, DDM = Dynamic Differential Microscopy [48], MSD = Mean Squared Displacement

DATA AND CODE AVAILABILITY

All data needed to evaluate the conclusions in the paper are present in the paper and/or the Supplementary Materials. All other data are available upon reasonable request to the authors.

Code for the Countoscope is available [67]. Code for computing the dynamic structure factor is also available [68].

ACKNOWLEDGEMENTS

We wish to acknowledge fruitful discussions with Jean-Louis Barrat, Roxanne Berthin, Ludovic Berthier, Roberto Cerbino, Benoit Coasne, Rafael Delgado Buscalioni, Aleksandar Donev, Simon Gravelle, Pierre Levitz, Grace Mattingly, Amaël Obliger and Alexander Schlaich.

Financial support for this project was provided by the Institute of Materials Science (iMAT) of the Alliance Sorbonne Université. A.C. acknowledges iMAT for a PhD grant. A.L.T. acknowledges funding from a Royal Society University Research Fellowship (URF\R1\211033). E.K.R.M. and A.L.T acknowledge funding from EPSRC (EP/X02492X/1). B.S. acknowledges funding from the National Science Foundation award DMS-2052515.

AUTHOR CONTRIBUTIONS

The authors confirm their contribution to the paper as follows: study conception and design: S.M.; simulation data collection: A.C.; simulation design: A.C., B.S.; experimental data collection: E.K.R.M.; experimental design: E.K.R.M., A.L.T., modeling: A.C., S.M.; data analysis: A.C.; data interpretation: A. C., B.S., A.L.T., S.M.; visualization: A.C.; draft manuscript preparation: A.C., S.M.; review and editing: A.C., A.L.T, S.M.

COMPETING INTERESTS

The authors declare no competing interests.

[1] Ariskina K, Galliéro G, Obliger A. Free volume model for transport in flexible kerogen of source rock's organic matter. The Journal of Physical Chemistry B. 2022;126(38):7409-17. Available from: https://pubs.acs.org/doi/10.1021/acs.jpcb.2c03970.

[2] Obliger A, Pellenq R, Ulm FJ, Coasne B. Free volume theory of hydrocarbon mixture transport in nanoporous materials. The Journal of Physical Chemistry Letters. 2016;7(19):3712-7. Available from: https://doi.org/10.1021/acs.jpclett.6b01684.

[3] Falk K, Coasne B, Pellenq R, Ulm FJ, Bocquet L. Subcontinuum mass transport of condensed hydrocarbons in nanoporous media. Nature communications. 2015;6(1):6949.

[4] Cates ME, Tailleur J. Motility-induced phase separation. Annu Rev Condens Matter Phys. 2015;6(1):219-44. Available from: https://www.annualreviews.org/content/journals/10.1146/annurev-conmatphys-031214-014710.

[5] Liebchen B, Marenduzzo D, Cates ME. Phoretic interactions generically induce dynamic clusters and wave patterns in active colloids. Physical review letters. 2017;118(26):268001. Available from: https://link.aps.org/doi/10.1103/PhysRevLett.118.268001.

[6] Liebchen B, Mukhopadhyay AK. Interactions in active colloids. Journal of Physics: Condensed Matter. 2021;34(8):083002. Available from: https://dx.doi.org/10.1088/1361-648X/ac3a86.

[7] Dijkstra M, Luijten E. From predictive modelling to machine learning and reverse engineering of colloidal self-assembly. Nature materials. 2021;20(6):762-73.

[8] Dhont JK. An introduction to dynamics of colloids. Elsevier; 1996.

[9] Einstein A. Über die von der molekularkinetischen Theorie der Wärme geforderte Bewegung von in ruhenden Flüssigkeiten suspendierten Teilchen. Annalen der physik. 1905;4.

[10] Schlaich A, Barrat JL, Coasne B. Theory and Modeling of Transport in Nanoporous Materials: From Microscopic to Coarse-Grained Descriptions. arXiv preprint arXiv:240603039. 2024. Available from: https://arxiv.org/abs/2406.03039.

[11] Pusey P. Liquids, Freezing and Glass Transition. Les Houches Session 51, 1989. 1991 Jan:765-942.

[12] Gomer R. Diffusion of adsorbates on metal surfaces. Reports on progress in Physics. 1990;53(7):917. Available from: https://dx.doi.org/10.1088/0034-4885/53/7/002.

[13] Panzuela S, Delgado-Buscalioni R. Solvent hydrodynamics enhances the collective diffusion of membrane lipids. Phys Rev Lett. 2018 Jul;121(4):048101. Available from: http://arxiv.org/abs/1803.03961.

[14] Panzuela S, Peláez RP, Delgado-Buscalioni R. Collective colloid diffusion under soft two-dimensional confinement. Phys Rev E. 2017 Jan;95(1):012602. Available from: https://link.aps.org/doi/10.1103/PhysRevE.95.012602.

[15] Kops-Werkhoven M, Fijnaut H. Dynamic behavior of silica dispersions studied near the optical matching point. The Journal of Chemical Physics. 1982;77(5):2242-53.

[16] Qiu X, Wu X, Xue J, Pine D, Weitz D, Chaikin PM. Hydrodynamic interactions in concentrated suspensions. Physical review letters. 1990;65(4):516.

[17] Segrè PN, Behrend OP, Pusey PN. Short-time Brownian motion in colloidal suspensions: Experiment and simulation. Physical Review E. 1995;52(5):5070. Available from: https://link.aps.org/doi/10.1103/PhysRevE.52.5070.

[18] Bleibel J, Domínguez A, Oettel M. 3D hydrodynamic interactions lead to divergences in 2D diffusion. J Phys: Condens Matter. 2015 apr;27(19):194113. Available from: https://dx.doi.org/10.1088/0953-8984/27/19/194113.

[19] Lin B, Rice SA, Weitz DA. Experimental evidence for the divergence of a transport coefficient in a quasi-two-dimensional fluid. Phys Rev E. 1995 jan;51(1):423-9. Available from: https://link.aps.org/doi/10.1103/PhysRevE.51.423.

[20] Lin B, Cui B, Xu X, Zangi R, Diamant H, Rice SA. Divergence of the long-wavelength collective diffusion coefficient in quasi-one- and quasi-two-dimensional colloidal suspensions. Phys Rev E. 2014 feb;89(2):022303. Available from: https://link.aps.org/doi/10.1103/PhysRevE.89.022303.

[21] Bleibel J, Domínguez A, Günther F, Harting J, Oettel M. Hydrodynamic interactions induce anomalous diffusion under partial confinement. Soft Matter. 2014 apr;10(17):2945-8. Available from: https://pubs.rsc.org/en/content/articlelanding/2014/sm/c3sm53043d.

[22] Falck E, Lahtinen JM, Vattulainen I, Ala-Nissila T. Influence of hydrodynamics on many-particle diffusion in 2D colloidal suspensions. Eur Phys J E. 2004 mar;13(3):267-75. Available from: https://doi.org/10.1140/epje/i2003-10075-9.

[23] Mackay EKR, Marbach S, Sprinkle B, Thorneywork AL. The Countoscope: Measuring Self and Collective Dynamics without Trajectories. Phys Rev X. 2024 Oct;14:041016. Available from: https://link.aps.org/doi/10.1103/PhysRevX.14.041016.

[24] Loussert C, Bouchaudy A, Salmon JB. Drying dynamics of a charged colloidal dispersion in a confined drop. Physical Review Fluids. 2016;1(8):084201. Available from: https://link.aps.org/doi/10.1103/PhysRevFluids.1.084201.

[25] Keita C, Hallez Y, Salmon JB. Microfluidic osmotic compression of a charge-stabilized colloidal dispersion: Equation of state and collective diffusion coefficient. Physical Review E. 2021;104(6):L062601. Available from: https://link.aps.org/doi/10.1103/PhysRevE.104.L062601.

[26] Sobac B, Dehaeck S, Bouchaudy A, Salmon JB. Collective diffusion coefficient of a charged colloidal dispersion: interferometric measurements in a drying drop. Soft matter. 2020;16(35):8213-25. Available from: https://pubs.rsc.org/en/content/articlelanding/2020/sm/d0sm00860e.

[27] Merlin A, Angly J, Daubersies L, Madeira C, Schöder S, Leng J, et al. Time-resolved microfocused small-angle X-ray scattering investigation of the microfluidic concentration of charged nanoparticles. The European Physical Journal E. 2011;34:1-7.

[28] Moisan L. Periodic plus smooth image decomposition. Journal of Mathematical Imaging and Vision. 2011;39:161-79.

[29] Giavazzi F, Edera P, Lu PJ, Cerbino R. Image windowing mitigates edge effects in Differential Dynamic Microscopy. The European Physical Journal E. 2017;40:1-9.

[30] Zuccolotto-Bernez A, Rojas-Ochoa L, Egelhaaf S, Escobedo-Sánchez M. Improving data sampling with rapid statistical convergence in digital Fourier microscopy analysis. Applied Optics. 2024;63(34):8760-70. Available from: https://opg.optica.org/ao/abstract.cfm?URI=ao-63-34-8760.

[31] Ala-Nissila T, Ferrando R, Ying S. Collective and single particle diffusion on surfaces. Advances in Physics. 2002;51(3):949-1078. Available from: https://doi.org/10.1080/00018730110107902.

[32] Thorneywork A. Structure and dynamics of two-dimensional colloidal hard spheres. University of Oxford; 2015.

[33] Thorneywork AL, Roth R, Aarts DGAL, Dullens RPA. Communication: Radial distribution functions in a two-dimensional binary colloidal hard sphere system. The Journal of Chemical Physics. 2014 apr;140(16):161106. Available from: https://doi.org/10.1063/1.4872365.

[34] Thorneywork AL, Rozas RE, Dullens RPA, Horbach J. Effect of Hydrodynamic Interactions on Self-Diffusion of Quasi-Two-Dimensional Colloidal Hard Spheres. Phys Rev Lett. 2015 Dec;115(26):268301. Available from: https://link.aps.org/doi/10.1103/PhysRevLett.115.268301.

[35] Crocker JC, Grier DG. Methods of Digital Video Microscopy for Colloidal Studies. Journal of Colloid and Interface Science. 1996 Apr;179(1):298-310. Available from: https://www.sciencedirect.com/science/article/pii/S0021979796902179.

[36] Allan DB, Caswell T, Keim NC, van der Wel CM, Verweij RW. soft-matter/trackpy: Trackpy v0.5.0. Zenodo; 2021.

[37] Sprinkle B, Van Der Wee EB, Luo Y, Driscoll MM, Donev A. Driven dynamics in dense suspensions of microrollers. Soft Matter. 2020;16(34):7982-8001. Available from: http://dx.doi.org/10.1039/D0SM00879F.

[38] Goldman AJ, Cox RG, Brenner H. Slow viscous motion of a sphere parallel to a plane wall—I Motion through a quiescent fluid. Chemical engineering science. 1967;22(4):637-51.

[39] Mackay EK, Young A, Carter A, Marbach S, Thorneywork AL. Static structure in interacting systems suppresses the influence of return kinetics on low frequency noise. to appear. 2024.

[40] Dean DS. Langevin equation for the density of a system of interacting Langevin processes. Journal of Physics A: Mathematical and General. 1996;29(24):L613. Available from: https://dx.doi.org/10.1088/0305-4470/29/24/001.

[41] Kawasaki K. Stochastic model of slow dynamics in supercooled liquids and dense colloidal suspensions. Physica A: Statistical Mechanics and its Applications. 1994;208(1):35-64. Available from: https://www.sciencedirect.com/science/article/pii/0378437194905339.

[42] Efron B. Bootstrap methods: another look at the jackknife. In: Breakthroughs in statistics: Methodology and distribution. Springer; 1992. p. 569-93. Available from: https://doi.org/10.1214/aos/1176344552.

[43] Sedlmeier F, Horinek D, Netz RR. Spatial Correlations of Density and Structural Fluctuations in Liquid Water: A Comparative Simulation Study. J Am Chem Soc. 2011 feb;133(5):1391-8. Available from: https://pubs.acs.org/doi/10.1021/ja1064137.

[44] Kellouai W, Barrat JL, Judeinstein P, Plazanet M, Coasne B. On De Gennes narrowing of fluids confined at the molecular scale in nanoporous materials. The Journal of Chemical Physics. 2024;160(2). Available from: https://doi.org/10.1063/5.0186956.

[45] Minh THN, Rotenberg B, Marbach S. Ionic fluctuations in finite volumes: fractional noise and hyperuniformity. Faraday Discussions. 2023. Available from: http://dx.doi.org/10.1039/D3FD00031A.

[46] Elson EL, Magde D. Fluorescence correlation spectroscopy. I. Conceptual basis and theory. Biopolymers: Original Research on Biomolecules. 1974;13(1):1-27. Available from: https://onlinelibrary.wiley.com/doi/abs/10.1002/bip.1974.360130102.

[47] Berne BJ, Pecora R. Dynamic light scattering: with applications to chemistry, biology, and physics. Courier Corporation; 2000.

[48] Cerbino R, Trappe V. Differential Dynamic Microscopy: Probing Wave Vector Dependent Dynamics with a Microscope. Phys Rev Lett. 2008 may;100(18):188102. Available from: https://link.aps.org/doi/10.1103/PhysRevLett.100.188102.

[49] Peláez RP, Usabiaga FB, Panzuela S, Xiao Q, Delgado-Buscalioni R, Donev A. Hydrodynamic fluctuations in quasi-two dimensional diffusion. J Stat Mech. 2018 jun;2018(6):063207. Available from: https://iopscience.iop.org/article/10.1088/1742-5468/aac2fb.

[50] Nägele G, Banchio AJ, Kollmann M, Pesché R. Dynamic properties, scaling and related freezing criteria of two- and three-dimensional colloidal dispersions. Molecular Physics. 2002 sep;100(18):2921-33. Available from: http://www.tandfonline.com/doi/abs/10.1080/00268970110109880.

[51] Pesché R, Nägele G. Stokesian dynamics study of quasi-two-dimensional suspensions confined between two parallel walls. Phys Rev E. 2000 oct;62(4):5432-43. Available from: https://link.aps.org/doi/10.1103/PhysRevE.62.5432.

[52] Hashemi A, Peláez RP, Natesh S, Sprinkle B, Maxian O, Gan Z, et al. Computing hydrodynamic interactions in confined doubly periodic geometries in linear time. The Journal of Chemical Physics. 2023 04;158(15):154101. Available from: https://doi.org/10.1063/5.0141371.

[53] Liron N, Mochon S. Stokes flow for a Stokeslet between two parallel flat plates. J Eng Math. 1976;10:287-303.

[54] Manzo C, Garcia-Parajo MF. A review of progress in single particle tracking: from methods to biophysical insights. Reports on progress in physics. 2015;78(12):124601. Available from: https://dx.doi.org/10.1088/0034-4885/78/12/124601.

[55] Deforet M, Parrini MC, Petitjean L, Biondini M, Buguin A, Camonis J, et al. Automated velocity mapping of migrating cell populations (AVeMap). Nature methods. 2012;9(11):1081-3.

[56] Hassan PA, Rana S, Verma G. Making Sense of Brownian Motion: Colloid Characterization by Dynamic Light Scattering. Langmuir. 2015;31(1):3-12. Available from: https://doi.org/10.1021/la501789z.

[57] Rose KA, Molaei M, Boyle MJ, Lee D, Crocker JC, Composto RJ. Particle tracking of nanoparticles in soft matter. Journal of Applied Physics. 2020;127(19).

[58] Zhang HP, Be'er A, Florin EL, Swinney HL. Collective motion and density fluctuations in bacterial colonies. Proceedings of the National Academy of Sciences. 2010;107(31):13626-30. Available from: https://www.pnas.org/doi/abs/10.1073/pnas.1001651107.

[59] Peruani F, Starruß J, Jakovljevic V, Søgaard-Andersen L, Deutsch A, Bär M. Collective Motion and Nonequilibrium Cluster Formation in Colonies of Gliding Bacteria. Phys Rev Lett. 2012 Feb;108:098102. Available from: https://link.aps.org/doi/10.1103/PhysRevLett.108.098102.

[60] Liu Z, Zeng W, Ma X, Cheng X. Density fluctuations and energy spectra of 3D bacterial suspensions. Soft Matter. 2021;17(48):10806-17. Available from: http://dx.doi.org/10.1039/D1SM01183A.

[61] Fily Y, Marchetti MC. Athermal Phase Separation of Self-Propelled Particles with No Alignment. Phys Rev Lett. 2012 Jun;108:235702. Available from: https://link.aps.org/doi/10.1103/PhysRevLett.108.235702.

[62] Alarcón F, Valeriani C, Pagonabarraga I. Morphology of clusters of attractive dry and wet self-propelled spherical particle suspensions. Soft matter. 2017;13(4):814-26. Available from: http://dx.doi.org/10.1039/C6SM01752E.

[63] Chaté H, Ginelli F, Grégoire G, Raynaud F. Collective motion of self-propelled particles interacting without cohesion. Physical Review E. 2008;77(4):046113. Available from: https://link.aps.org/doi/10.1103/PhysRevE.77.046113.

[64] Fadda F, Matoz-Fernandez DA, van Roij R, Jabbari-Farouji S. The interplay between chemo-phoretic interactions and crowding in active colloids. Soft Matter. 2023;19(13):2297-310. Available from: http://dx.doi.

org/10.1039/D2SM00957A.

[65] Narayan V, Ramaswamy S, Menon N. Long-lived giant number fluctuations in a swarming granular nematic. Science. 2007;317(5834):105-8. Available from: https://www.science.org/doi/abs/10.1126/science.1140414.

[66] Toner J, Tu Y, Ramaswamy S. Hydrodynamics and phases of flocks. Annals of Physics. 2005;318(1):170-244. Available from: https://www.sciencedirect.com/science/article/pii/S0003491605000540.

[67] Marbach S, Carter A, Sprinkle B. Countoscope/countoscope_PRX: v1.0.1. Zenodo; 2025. Available from: https://doi.org/10.5281/zenodo.15000583.

[68] Carter A. adamrobcarter/scattering_functions: v0.1.1. Zenodo; 2025. Available from: https://doi.org/10.5281/zenodo.14999376.

DATA AND CODE AVAILABILITY

All data needed to evaluate the conclusions in the paper are present in the paper and/or the Supplementary Materials. All other data are available upon reasonable request to the authors.

Code for the Countoscope is available [67]. Code for computing the dynamic structure factor is also available [68].

136x62mm (144 x 144 DPI)